

# Comparison of Phase Velocities from Array Measurements of Rayleigh Waves Associated with Microtremor and Results Calculated from Borehole Shear-Wave Velocity Profiles

by Hsi-Ping Liu, David M. Boore, William B. Joyner, David H. Oppenheimer, Richard E. Warrick, Wenbo Zhang,\* John C. Hamilton, and Leo T. Brown†

**Abstract** Shear-wave velocities ( $V_S$ ) are widely used for earthquake ground-motion site characterization.  $V_S$  data are now largely obtained using borehole methods. Drilling holes, however, is expensive. Nonintrusive surface methods are inexpensive for obtaining  $V_S$  information, but not many comparisons with direct borehole measurements have been published. Because different assumptions are used in data interpretation of each surface method and public safety is involved in site characterization for engineering structures, it is important to validate the surface methods by additional comparisons with borehole measurements. We compare results obtained from a particular surface method (array measurement of surface waves associated with microtremor) with results obtained from borehole methods. Using a 10-element nested-triangular array of 100-m aperture, we measured surface-wave phase velocities at two California sites, Garner Valley near Hemet and Hollister Municipal Airport. The Garner Valley site is located at an ancient lake bed where water-saturated sediment overlies decomposed granite on top of granite bedrock. Our array was deployed at a location where seismic velocities had been determined to a depth of 500 m by borehole methods. At Hollister, where the near-surface sediment consists of clay, sand, and gravel, we determined phase velocities using an array located close to a 60-m deep borehole where downhole velocity logs already exist. Because we want to assess the measurements uncomplicated by uncertainties introduced by the inversion process, we compare our phase-velocity results with the borehole  $V_S$  depth profile by calculating fundamental-mode Rayleigh-wave phase velocities from an earth model constructed from the borehole data. For wavelengths less than  $\sim 2$  times of the array aperture at Garner Valley, phase-velocity results from array measurements agree with the calculated Rayleigh-wave velocities to better than 11%. Measurement errors become larger for wavelengths 2 times greater than the array aperture. At Hollister, the measured phase velocity at 3.9 Hz (near the upper edge of the microtremor frequency band) is within 20% of the calculated Rayleigh-wave velocity. Because shear-wave velocity is the predominant factor controlling Rayleigh-wave phase velocities, the comparisons suggest that this nonintrusive method can provide  $V_S$  information adequate for ground-motion estimation.

## Introduction

Shear-wave velocity information in soil and rock are widely used in earthquake engineering (e.g., Kramer, 1996). For instance, for empirical prediction of strong ground mo-

tion (e.g., Boore *et al.*, 1997) and site coefficients for building codes (NEHRP 1997; ICBO 1997), for liquefaction potential characterization (e.g., Stokoe and Nazarian, 1985), for embankment stability analysis (e.g., Charlie *et al.*, 1985), and as input for numerical simulation of basin response (e.g., Graves, 1998).

$V_S$  data are now largely obtained using borehole methods. However, the drilling and cuttings disposal costs for

\*Present address: Beijing Strong-Motion Observation Center, Institute of Engineering Mechanics, China Seismological Bureau, Beijing 100080, China

†Present address: Geovision Geophysical Services, 1785 Pomona Road, Suite B, Corona, California 92880

these methods are high. Compared to direct borehole methods, nonintrusive surface methods for obtaining  $V_S$  information cost much less. Such surface methods include refraction and inversion of Rayleigh-wave phase velocities using controlled sources [e.g., the Spectral-Analysis-of-Surface-Waves (SASW) method, Stokoe *et al.*, 1994], explosions (e.g., Malagnini *et al.*, 1997), or microtremor (e.g., Horike, 1985; Milana *et al.*, 1996; Kawase *et al.*, 1998). Because different assumptions are used in data interpretation of each surface method, and each method has its own limitations, it is important to validate the surface methods by additional comparisons with borehole measurements. More comparisons are also required from a practical point of view because public safety is involved in site characterization for engineering structures.

There have been a few comparisons of the SASW method with borehole measurements (Stokoe and Nazarian, 1985; Brown, 1998; Brown *et al.*, 2000). The purpose of this article is to compare velocity results obtained from another surface method, array measurements of surface waves associated with microtremor, with those obtained from borehole methods. Because we want to assess the measurements uncomplicated by uncertainties introduced by the inversion process, we have chosen to use phase velocities as the basis for comparison rather than the shear-wave velocities obtained by inverting the phase velocities. A complete assessment of shear-wave velocities obtained from surface-wave methods would, of course, require consideration of the uncertainties introduced by inversion.

We have conducted array measurements at two California sites where borehole velocity data already exist. The two sites are located at Garner Valley near Hemet (where borehole velocities have been determined to a depth of 500 m) and at Hollister Municipal Airport (where borehole velocities have been determined to a depth of 60 m). We first describe the experiments and results for the two sites. Results of numerical simulations for the Garner Valley site using synthetic ground noise are discussed in an Appendix.

## Garner Valley

### Site and Array Location

Figure 1 shows the location of the 100-m aperture array. The site is located on an ancient lake bed where water-saturated sediment (20-m thick) overlies decomposed granite (67-m thick) on top of the granite bedrock (Steidl *et al.*, 1996). Seismic velocities at the site have been measured using borehole suspension loggers to 500-m depth. In addition, interval velocities have been determined from earthquake arrival times at a 6-level three-component borehole accelerometer array; the deepest accelerometer is located at a depth of 220 m and the surface projection of the 6-level vertical array is covered by our array. Figure 2 shows the  $V_S$  structure and geologic log of the site (Jamison H. Steidl, University of California at Santa Barbara, 1997, written

communication). The sources of microtremor are presumably traffic on local highways and in the local campgrounds.

### Experimental Arrangement

The array consists of ten Mark Products Model L-4C 1 Hz vertical-component geophones, calibrated and adjusted to 0.7 of critical damping.

Prior to field experiments, we estimated the error in phase-velocity measurement due to differences in geophone phase characteristics by the following procedure. Geophones were compared in pairs by placing two geophones side-by-side on the floor of our basement laboratory. We recorded ground noise for 60 seconds and then compute the Fourier phase spectrum of the records. At frequency  $f$  a phase difference,  $(\Delta\phi)_{ij}$ , between the phase spectrum of geophone  $i$  and of geophone  $j$  is equivalent to a time error in velocity measurement of  $(\Delta t)_{ij} = (\Delta\phi)_{ij}/(2\pi f)$ . In order to estimate the fractional error in phase velocity measured by an array, we approximate  $|\Delta c/c|_{\text{ave}} = |\Delta t/t|_{\text{ave}}$  by  $c|\Delta\phi|_{\text{ave}}/(2\pi f l_{\text{ave}})$  at frequency  $f$ , where  $|\Delta\phi|_{\text{ave}}$  is the average value of measured  $|(\Delta\phi)_{ij}|$ ,  $l_{\text{ave}}$  is the average separation between geophone pairs. For our experiment,  $|\Delta\phi|_{\text{ave}} = 4.2 \times 10^{-2}$  radians at 1 Hz,  $l_{\text{ave}} \cong 49$  m,  $c \cong 1.3$  km/sec, and therefore  $|\Delta c/c|_{\text{ave}} = 0.18$  at 1 Hz. Because in general  $c$  decreases with increasing  $f$ , this fractional error decreases at higher frequencies. We analyze our field data only for frequencies greater than or equal to 1 Hz.

In the field, we laid out the geophones in a nested-triangular configuration using an electronic total station to control sensor location. Position error, introduced when geophones were emplaced in soil, is  $\pm 2$  cm. The nested-triangular configuration, shown in Figure 1, is representative of all our arrays.

Each geophone was hard-wired to one of two digital recorders. Sampling rate was set at 200 samples/sec, and the low-pass filter cutoff frequency was set at 33 Hz. Timing of the two recorders, controlled by an external clock, was synchronized to better than 0.1 msec.

Details of the field experimental arrangement are given in Liu *et al.* (2000).

### Microtremor Measurements

Measurements were made on 24 June 1997 between 3:47 p.m. and 7:53 p.m. local time (97:175:22:47 to 97:176:02:53 UTC). The time period was chosen because microtremor of car traffic decreased by an order of magnitude after 10 p.m.

### Data

Figure 3a shows microtremor recorded by the Garner Valley array at 4:22 p.m. on 24 June 1997; these microtremor records are very similar to each other. In contrast, the microtremor shown in Figure 3b, recorded at 6:17 p.m. on the same day, are less similar to each other. Fourier spectra of the microtremor in Figure 3 are shown in Figure 4 and discussed in the Results section below.

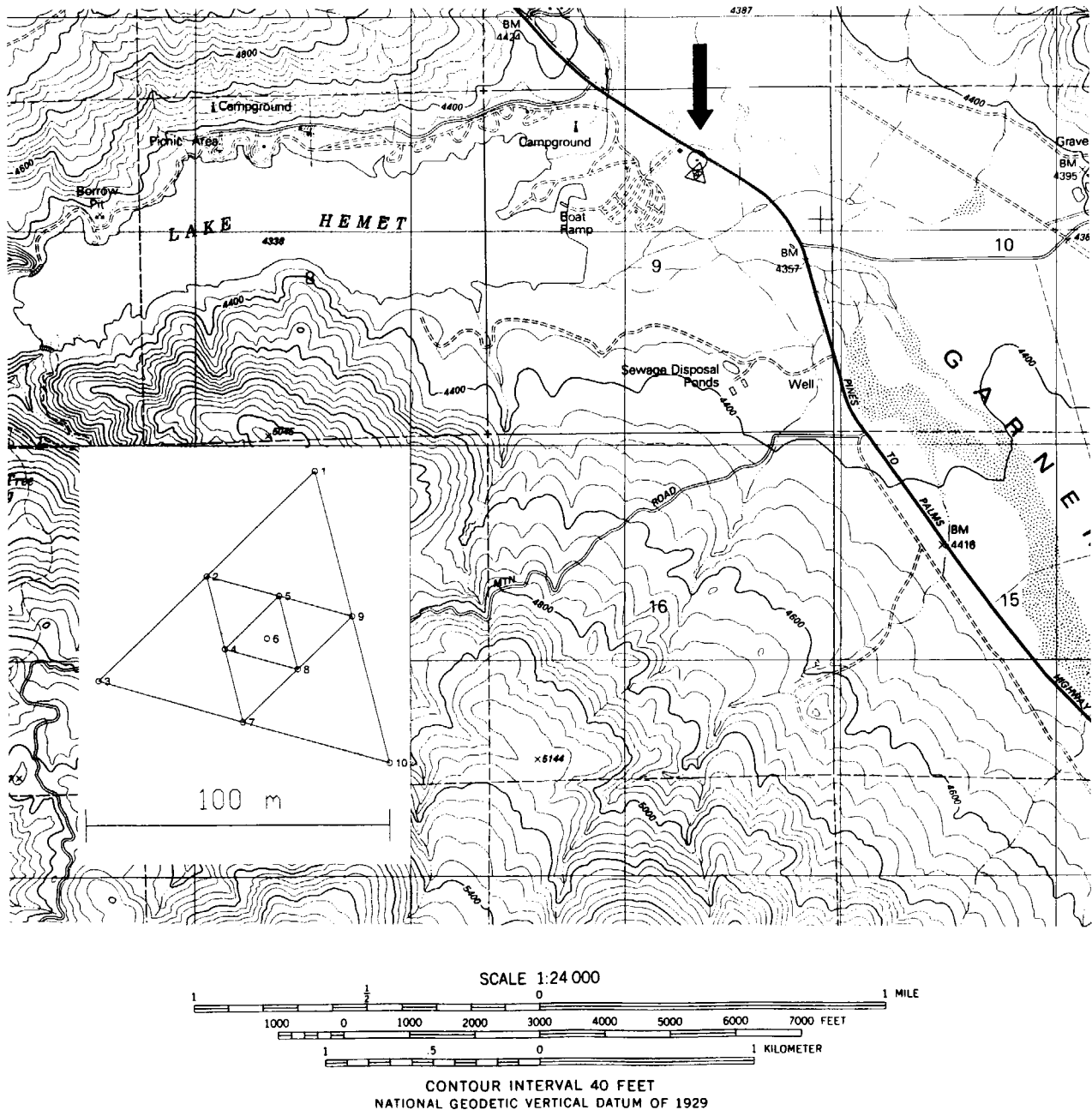


Figure 1. Array location at the Garner Valley site; an arrow points to the 100-m aperture array and a dot in a circle locates the 500-m-deep borehole. The array configuration is shown in the insert.

### Data Analysis

Array analysis of seismic data are discussed in, e.g., Capon *et al.* (1967), Lacoss *et al.* (1969), Capon (1969, 1973), and Aki and Richards (1980, pp. 619–625). We have analyzed our data from 2.4 to 5.9 Hz using the high-resolution frequency wavenumber spectrum-analysis method of Capon *et al.* (1967) with computer codes similar to those used by Liaw (1977) and Oppenheimer and Iyer (1980). Details of implementation of the analysis method are given in Liu *et al.* (2000).

### Results

*Fourier Spectra.* Figures 4a and 4b show the Fourier spectra of the microtremor shown in Figures 3a and 3b, respectively. These spectra have significant amplitudes from  $\sim 5$  Hz to beyond 10 Hz. Reflecting the microtremor records of Figure 3, the spectra in Figure 4a are quite similar to each other, whereas in contrast, those in Figure 4b are less similar to each other. There are obvious differences among the velocity spectra shown in Figure 4b, that is, between those of station #3 and station #10. One possible cause for these dif-

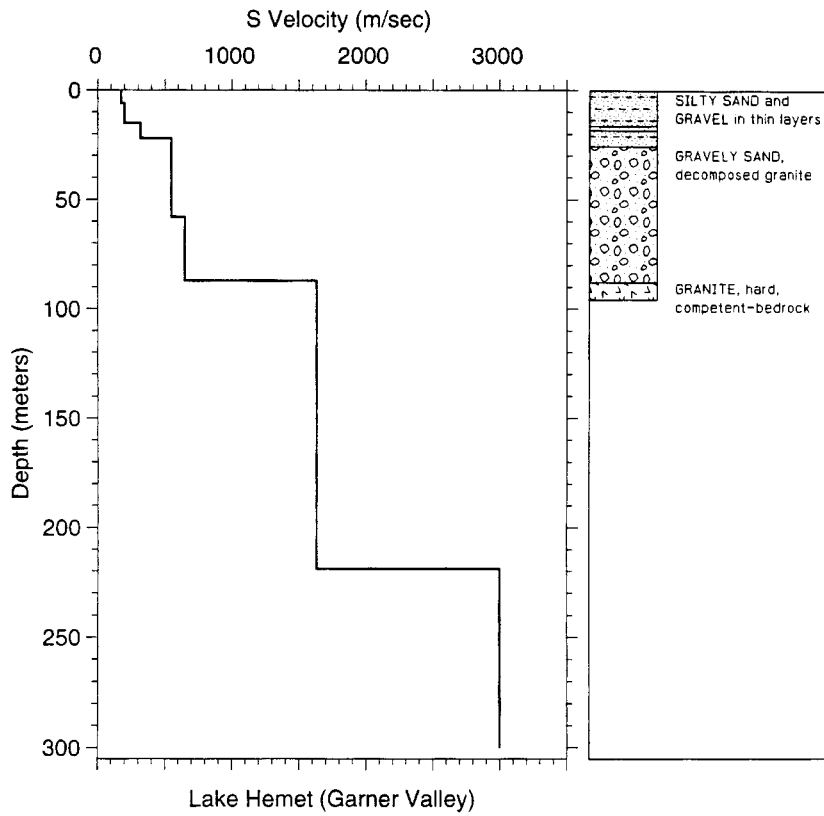
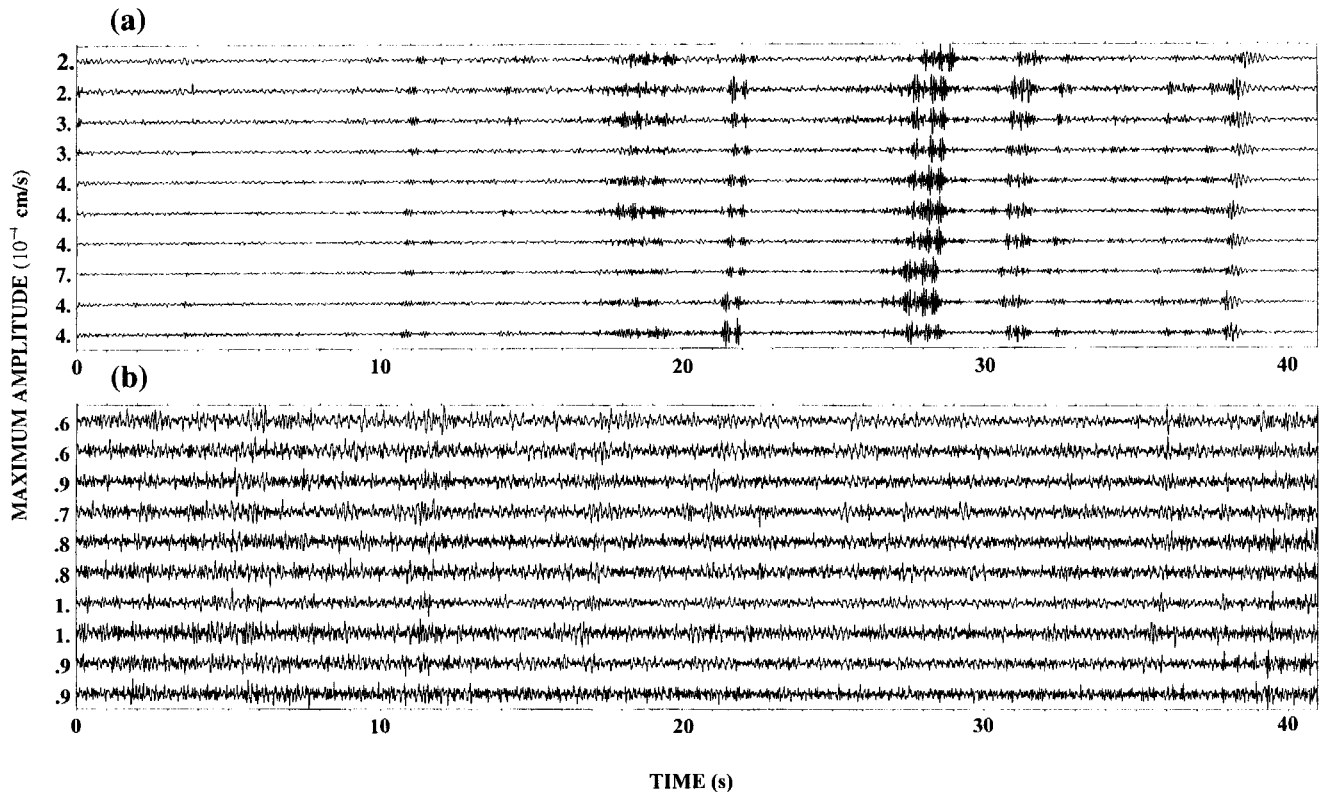


Figure 2. Shear-wave velocities and simplified geologic log of the Garner Valley site.



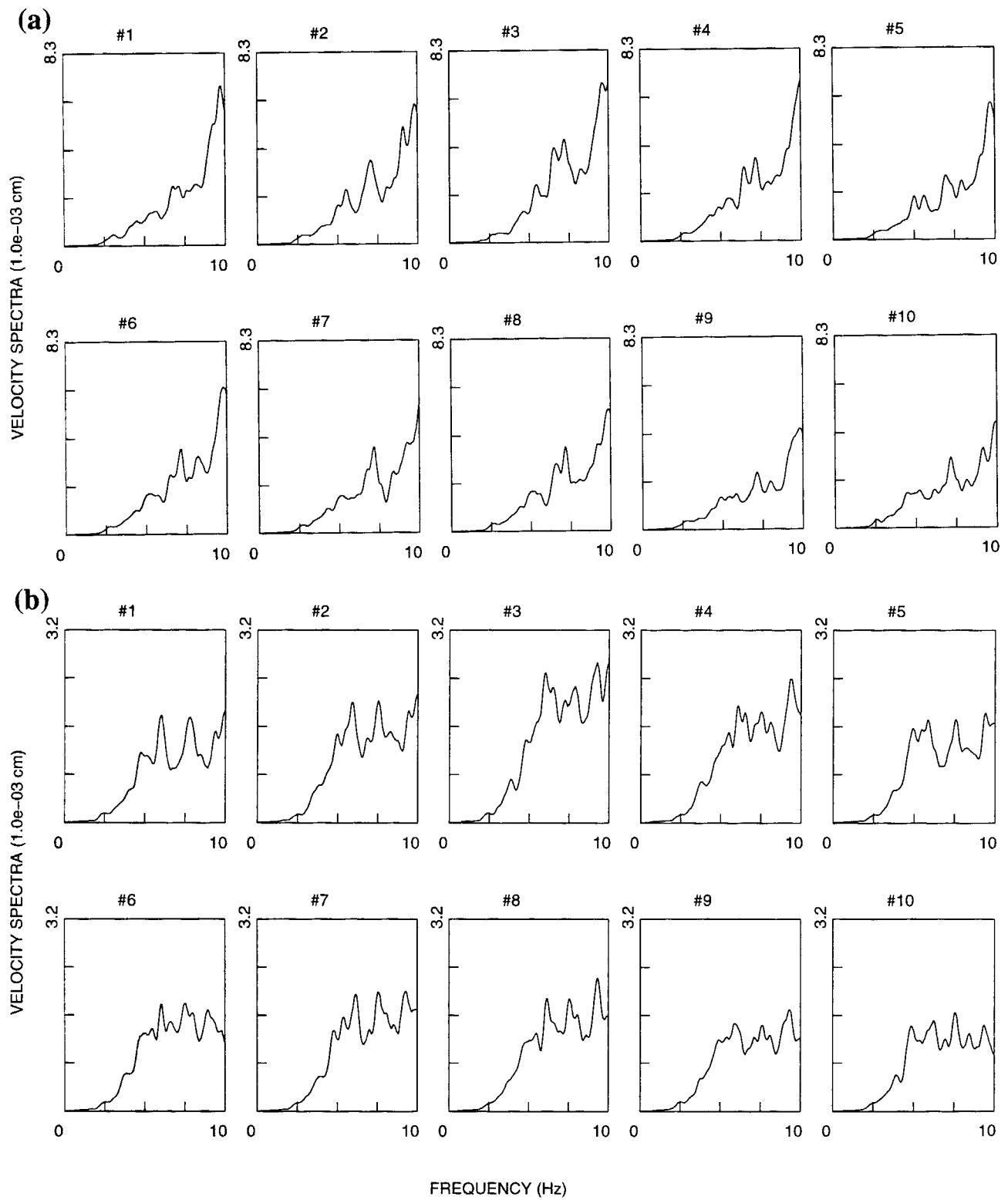


Figure 4. (a) Fourier spectra of the microtremor records obtained by the Garner-Valley array shown in Figure 3a, and (b) Fourier spectra of the microtremor records shown in Figure 3b.

ferences is the incoherent noise generated by wind action on vegetation (Capon, 1973). However, because the wind was dying down when the data were obtained, it is likely that these differences are caused by interference from multiazimuth surface waves. The consequences of this interference depend on the relative strength and location of the sources which can be time variable.

**Power-Spectrum Contours.** Figure 5a shows  $|P(s_x, s_y, \omega)|$  at 4.6 Hz from the microtremor records shown in Figure 3a, where  $P(s_x, s_y, \omega)$  is the power output of the array process filter as a function of wave-slowness components  $s_x$  and  $s_y$  for a specific angular frequency  $\omega$ . Two contour peaks are resolved with the highest peak at a back azimuth of  $291.5^\circ$ . In contrast, the plot for  $|P(s_x, s_y, \omega)|$  at the same frequency for the microtremor records of Figure 3b, shown in Figure 5b, displays five resolved peaks. These power-spectrum contours substantiate our interpretation that the lack of similarity among the spectra in Figure 4b as compared to those in Figure 4a is caused by multiazimuth surface waves.

**Phase Velocity and Backazimuth Results from Field Measurements: Comparison of Velocity Results with Calculated Rayleigh-Wave Velocities Based on Earth Models Constructed from Borehole Logs and Earthquake Data.** For each  $|P(s_x, s_y, \omega)|$  contour plot derived from a suite of microtremor records of 40.96-sec duration from 10 geophones, we determine the phase velocity and backazimuth given by the highest contour peak. Phase velocities from 2.4 to 5.9 Hz from 31 measurements are shown in Figure 6. Light error bar represents  $\pm 1$  standard deviation of the phase velocity and heavy error bar represents  $\pm 1$  standard error of the mean. The error-bar size increases at low frequencies.

Also shown in Figure 6 are phase velocities determined by the SASW method (Stokoe *et al.*, 1994; Brown, 1998).

A Rayleigh-wave fundamental mode velocity-dispersion curve calculated from an earth model constructed from borehole logging data and earthquake arrival times is also shown in Figure 6. ( $V_S$  of this earth model is shown in Figure 2.) The measured phase velocities agree with the calculated value to better than 11% above 3.4 Hz.

Figure 7 shows the backazimuth of the highest peak of all the analyzed contour plots. There are 31 backazimuth values at each frequency, corresponding to the 31 separate time segments used in our data analysis. The back azimuths cluster in two groups, one centered around  $\sim 145^\circ$  and the other  $\sim 280^\circ$ . These results are consistent with traffic sources on the Palms to Pines Highway and in the Lake Hemet Campground.

## Hollister Municipal Airport

### Site and Array Locations

Figure 8 shows the location of a 100-m aperture array and a nearby borehole ( $\sim 70$  m from the northeast array tip) where velocity logs to a depth of 60 m had been obtained

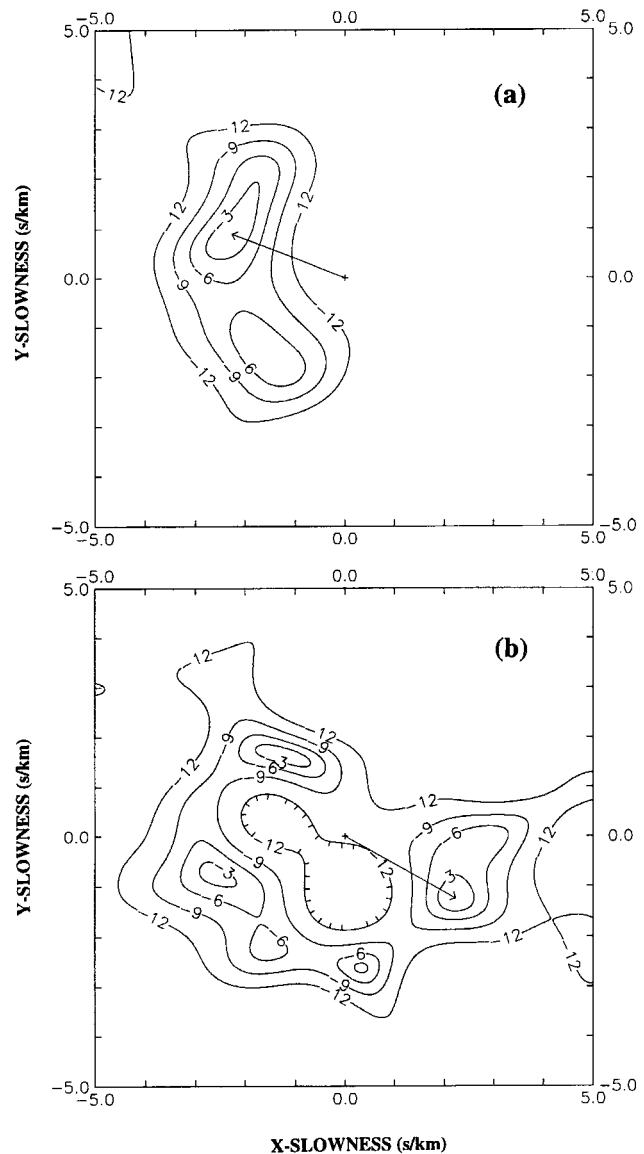


Figure 5. (a) Contour plot of  $|P(s_x, s_y, \omega)|$  at 4.6 Hz for microtremor records shown in Figure 3a. Two contour peaks are resolved with the highest peak at a back azimuth of  $291.5^\circ$ . (b) Contour plot of  $|P(s_x, s_y, \omega)|$  at 4.6 Hz for microtremor records shown in Figure 3b. In contrast to (a), five resolved peaks are displayed.

(Gibbs and Fumal, 1994). Figure 9 shows the  $V_S$  and geologic logs from the borehole. The sediment consists of clay, sand, gravelly sand, and sandy gravel layers. Kilburn (1972) gives additional geologic information from well logs of four deep oil and gas test holes. (The closest of these four holes, the V. I. Gandrup, O'Connell No. 1, is located at  $\sim 1.4$  km northeast of the 60 m borehole mentioned previously, see Figure 8). The unconsolidated or poorly consolidated Tertiary or Quaternary units in increasing depth are (1)  $\sim 310$  m of alluvium, old alluvium, San Benito gravel, and alluvial-fan material from the Diablo Range; (2) three or four thick

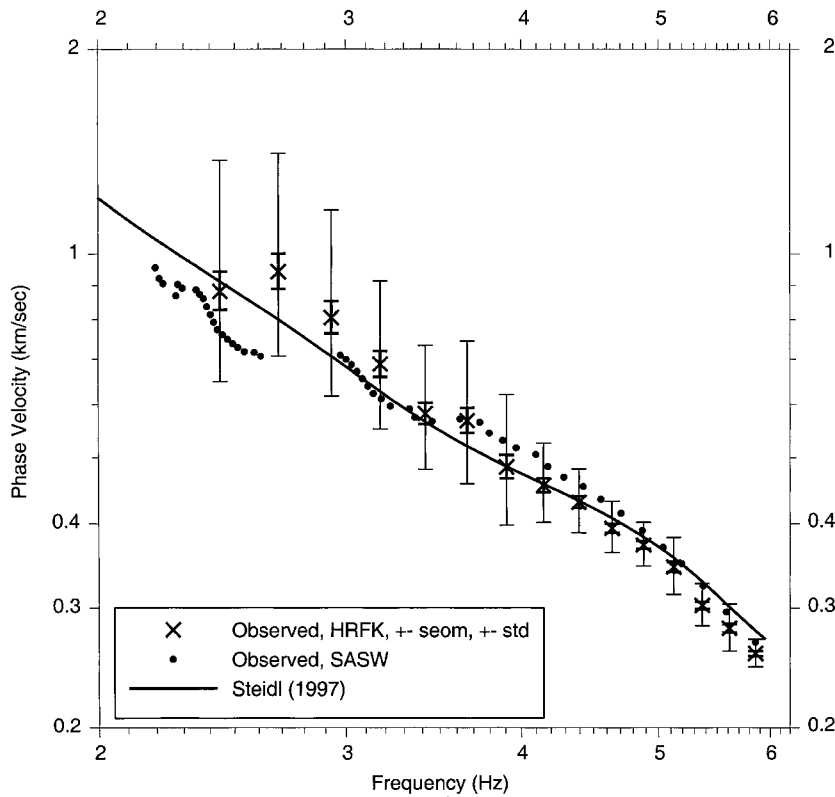


Figure 6. Phase velocities obtained from 31 separate time segments of the Garner-Valley array using the high-resolution-frequency-wavenumber (HRFK) spectrum-analysis method and a velocity-dispersion curve calculated from an earth model (see Figure 2). Light error bar represents  $\pm 1$  standard deviation (std) of the phase velocity; heavy error bar represents  $\pm 1$  standard error of the mean (seom). Phase velocities obtained at the same site by the SASW method (Brown, 1998) are also included for comparison.

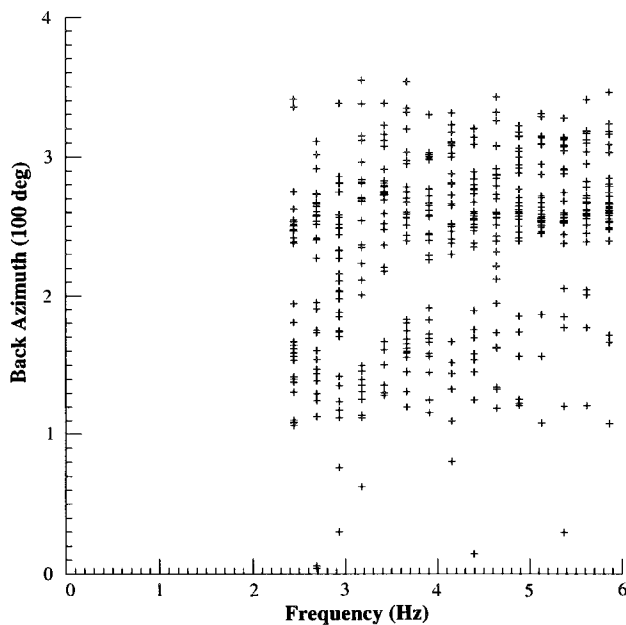


Figure 7. Back azimuth of the highest peak of contour plots from 31 separate time segments recorded by the Garner-Valley array.

sand sequences separated by thinner clay intervals, totaling  $\sim 520$  m; and (3) clay, sand, and gravel totaling  $\sim 370$  m. What is described as consolidated bedrock in the Gandrup well is encountered at  $\sim 1200$ -m depth.

This site is suitable for array measurement of surface waves associated with microtremor in that the traffic sources on the surrounding highways are sufficiently far-off that the microtremor produced by the traffic sources is predominantly surface waves.

#### Experimental Arrangement

The experimental arrangement is similar to that at the Garner Valley site except that the digital recorder low-pass filter cutoff frequency was set at 50 Hz.

#### Microtremor Measurements

Measurements were conducted from 3:54 p.m., 10 October to 7:09 a.m., 11 October 1996, local time (96:284:22:54 to 96:285:14:09 UTC). The time period was chosen when activities within the airport decreased and then stopped almost completely after dark. Microtremor was monitored and records were taken for many  $\sim 60$ -sec segments.

#### Data Analysis and Results

We have analyzed our field data using the same procedure as that for the Garner Valley data.

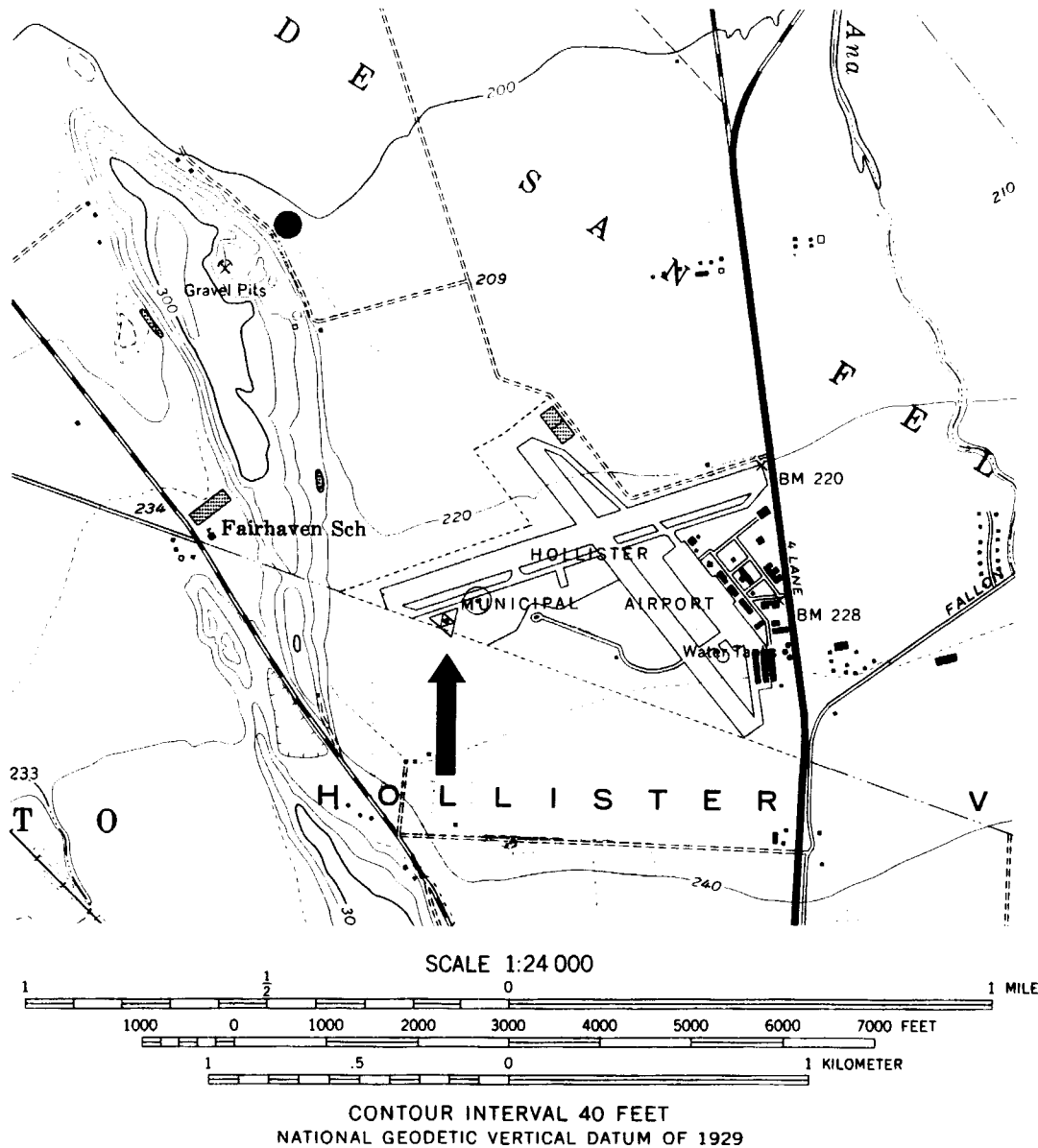


Figure 8. The array location at the Hollister Municipal Airport (pointed by an arrow), and location of the 60-m-deep borehole (dot with a circle) where downhole velocity logs were obtained. A solid circle near a pressure ridge of the Calaveras fault indicates an oil and gas test well that reached bedrock at ~1,200-m depth.

*Phase Velocities and Comparison with Rayleigh-Wave Velocities Calculated from Earth Models Constructed from Borehole Logs.* Phase velocities determined from 67 separate time segments and for frequencies from 1.0 to 3.9 Hz are shown in Figure 10 with five velocity-dispersion curves.

Curve #1 is that for Rayleigh waves of the fundamental mode calculated from an earth model constructed using the 60-m deep borehole logging data and a half-space extending downward from the borehole bottom, velocities of the half-space are assumed to be those at the borehole bottom. This relatively flat curve fits poorly to our observation for frequencies less than 3 Hz because the low  $V_S$  value of 388 m/

sec. assumed for the half-space is clearly inappropriate for the entire sedimentary sequence from 60 m to ~1200 m.

Curve #2 is calculated using an earth model constructed from the borehole logs for the top 60 meters and estimated for the lower depths to 1160 m guided by the geologic information from Kilburn (1972). Extrapolations for  $V_S$  from 60 m to 1160 m are based on the equation,

$$V_S = V_{S0} (z/z_0)^{0.25}. \tag{1}$$

By choosing  $V_{S0} = 400$  m/sec at  $z_0 = 60$  m, we obtain a subjectively chosen lower bound consistent with the mea-

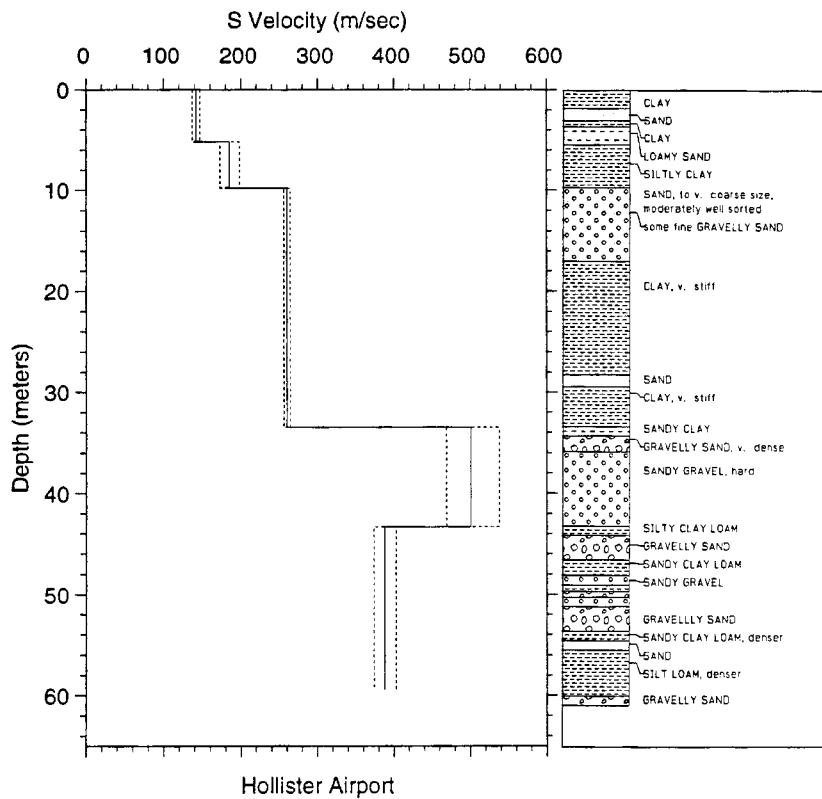


Figure 9. Shear-wave-velocity profiles (light dashed lines representing plus and minus one standard deviation) and simplified geologic log obtained from a borehole at the Hollister Municipal Airport ~70 m from the north-east tip of our array.

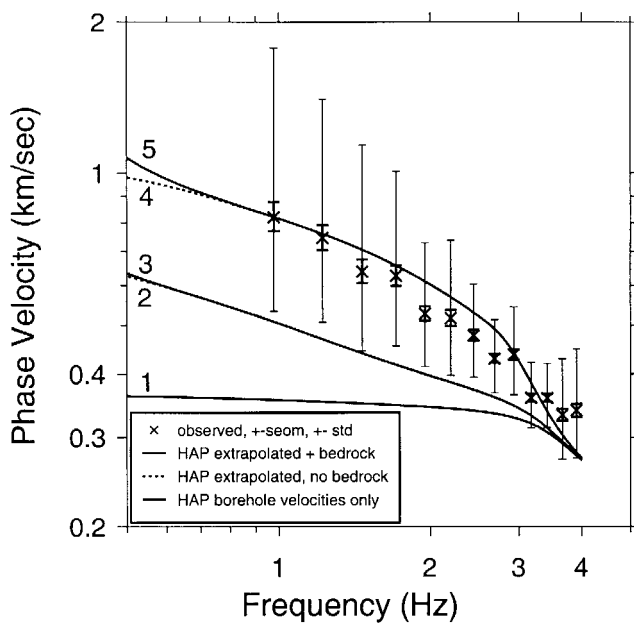


Figure 10. Phase velocities determined from 67 separate time segments (light error bar represents  $\pm 1$  standard deviation of the phase velocity and heavy error bar represents  $\pm 1$  standard deviation of the mean). The dispersion curves are calculated from earth models constructed from borehole logging data and site geologic information (see text). Dispersion curve #2 is barely visible because of our choice of 0.5 Hz as the lower limit of the frequency axis.

sured velocities in the top 60 m. The continuous model from equation (1) is then used to construct a constant-velocity layered model under the condition that the layered and continuous model yield the same travel time across each layer. Velocity of the bottom layer is also assumed for the bedrock below 1160 m. (See model #2 in Figure 11.) We obtain curve #3 by using the more appropriate bedrock velocities [ $V_S = 2.0$  km/sec and  $V_P = 4.0$  km/sec, guided by Yamamizu and Goto (1978) and Yamamizu *et al.* (1981)] in the earth model for curve #2.

Curves #4 and #5 are calculated when the  $V_S$  estimation for unconsolidated or poorly consolidated materials from 60 m to 1160 m is a subjectively chosen upper bound consistent with the measured velocities in the top 60 m (using  $V_{S0} = 600$  m/sec at  $z_0 = 60$  m in equation 1). Velocity of the material at 1160 m is assumed for the bedrock in the model for curve #4 whereas  $V_S = 2.0$  km/sec and  $V_P = 4.0$  km/sec were used as bedrock velocities for curve #5.

The calculated phase velocities at 3.9 Hz from all models, however, are essentially the same (indicating that phase velocity is not influenced significantly by layers deeper than 60 m) and are within 20% of the measured phase velocity. Curves #2, #3, #4, and #5 show that the bedrock is sufficiently deep that the bedrock velocities have negligible effect on phase velocities for frequencies greater than or equal to 1 Hz. Generally, the measured phase velocities fall within the dispersion curves calculated using the estimated lower and upper bounds of the velocity profile.

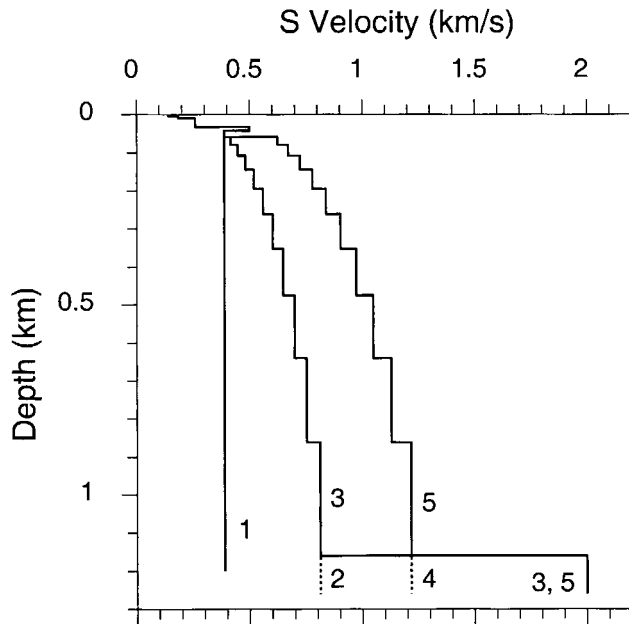


Figure 11.  $V_S$  models for calculating fundamental-mode Rayleigh-wave dispersion curves in Figure 10.  $V_S$  for the top 60 m are obtained from the borehole logging data (see Figure 9).  $V_S$  estimates for lower depths to 1160 m (a lower estimate to the left and an upper estimate to the right) are guided by the geologic information from Kilburn (1972) and the velocity information from Yamamizu and Goto (1978) and Yamamizu *et al.* (1981). Bedrock  $V_S$  is estimated to be 2.0 km/sec.

### Discussion and Conclusions

We have measured the phase velocities of surface waves associated with microtremor at two California sites using surface arrays.

In order to compare a  $V_S$  depth profile from borehole methods with our phase-velocity results, we calculate the fundamental-mode Rayleigh-wave phase velocities from an earth model constructed from the borehole data. The alternative comparison by inverting our phase-velocity results to obtain a  $V_S$  depth profile would involve additional uncertainties introduced by the inversion process.

The simpler geologic conditions at Garner Valley and a velocity structure determined by borehole methods to 500-m in granite allow a meaningful comparison of measured phase velocities with the dispersion curve calculated from the velocity structure. We found that observations agree with borehole results to better than 11% except when the wavelength is greater than 2 times the array aperture, in which case the observations have increased scatter and are biased high relative to the dispersion curve.

At Hollister Airport, where we have velocity data only to 60-m depth, the phase velocity at 3.9 Hz (near the upper edge of the microtremor frequency band) is not influenced

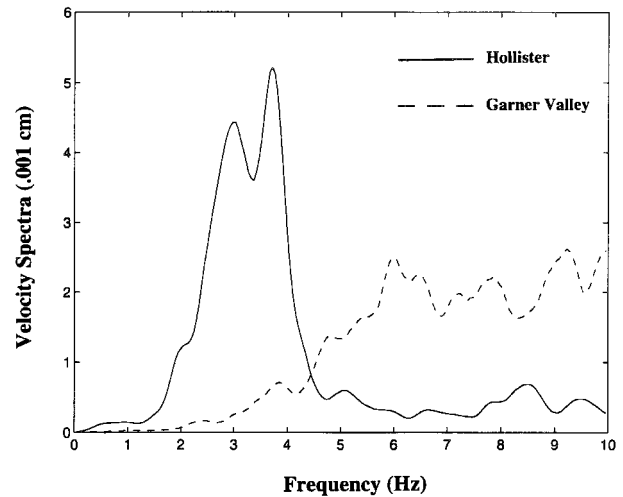


Figure 12. Comparison of microtremor spectra observed at Garner Valley and at Hollister. The Garner Valley spectrum has higher frequency content.

significantly by layers deeper than 60 m. The phase velocity measured by a 100-m array  $\sim 70$  m from the borehole is within 20% of the calculated Rayleigh-wave velocity. At lower frequencies, the measured phase velocities generally fall within the dispersion curves calculated using the estimated lower and upper bounds of the velocity profile.

Compared to surface methods using controlled sources and explosions, the present method is convenient because no source is required from the experimenter. For correct results, however, the microtremor sources, usually highway traffic, must be located sufficiently far away that the motion at the array is predominantly surface waves. Because microtremor is time- and site-dependent, in some places the frequency band of ground noise may not cover the frequencies of interest. Figure 12 shows the difference in microtremor spectra at the two sites of this study.

Because shear-wave velocity is the predominant factor controlling Rayleigh-wave phase velocities, surface-wave methods can provide  $V_S$  information adequate for ground-motion estimation. The agreement of results from this non-intrusive method and those obtained from borehole measurements, particularly at Garner Valley, gives us confidence in the microtremor method for ground motion estimation and site characterization.

### Acknowledgments

We thank Dr. Hiroshi Kawase who helped us with discussions during the course of this work and carefully reviewed our manuscript, Professor Kojiro Irikura and Dr. Hiroshi Kawase who kindly showed one of us (H.-P.L.) their field-work procedure in the San Fernando Valley of California; Mr. Allen Ritter, manager of Hollister Municipal Airport, California, for providing a field test site; Mr. Thomas E. Fumal, who directed us to the geologic information of Hollister based on deep oil and gas test wells; Mr. Robert V. Lindquist, Jr., General Manager of Lake Hemet Municipal Water

District, for permission to conduct tests at Garner Valley, California; Mr. Scott Swain for assistance in the field work at Garner Valley; Dr. Jamison H. Steidl for providing a Garner Valley earth model; Professor Robert B. Herrmann for providing surface-wave computer programs (Herrmann, 1996); and Drs. Arthur F. McGarr, Ken Miyakoshi, Jose M. Roesset, and James C. Savage, whose reviews improved our manuscript. This work is performed as a cooperative project between the U.S. Geological Survey and the U.S. Nuclear Regulatory Commission. Use of commercial product name (Mark Products) does not imply endorsement by the U.S. Geological Survey.

## References

- Aki, K., and P. G. Richards (1980). *Quantitative Seismology*, W. H. Freeman and Co., San Francisco, California.
- Boore, D. M., W. B. Joyner, and T. E. Fumal (1997). Equations for estimating horizontal response spectra and peak acceleration from Western North American earthquakes: a summary of recent work, *Seism. Res. Lett.* **68**, 128–153.
- Brown, L. T. (1998). Comparison of  $V_s$  profiles from SASW and borehole measurements at strong motion sites in southern California: *M. S. Thesis*, University of Texas, Austin, 349 pp.
- Brown, L. T., D. M. Boore, and K. H. Stokoe, II (2000). Comparison of shear-wave velocity profiles from SASW and downhole seismic tests at a strong-motion site, in Proc. 12th World Conference on Earthquake Engineering, Auckland, New Zealand, 30 January–4 February, 2000 (in press).
- Capon, J. (1969). High-resolution frequency-wavenumber spectrum analysis, *Proc. IEEE* **57**, 1408–1418.
- Capon, J. (1973). Signal processing and frequency-wavenumber spectrum analysis for a large aperture seismic array, in *Methods in Computational Physics: Geophysics*, B. A. Bolt, (Editor) Vol. 13, Academic Press, New York, 1–59.
- Capon, J., R. J. Greenfield, and R. J. Kolker (1967). Multidimensional maximum-likelihood processing of a large aperture seismic array, *Proc. IEEE* **55**, 192–211.
- Charlie, W. A., G. T. Jirak, and D. O. Doehring (1985). Seismic analysis of Horse Creek Dam, Hudson, Colorado, in *Proc. Conf. on Measurement and Use of Shear Wave Velocity for Evaluating Dynamic Soil Properties*, Denver, Colorado, 1 May 1985, R. D. Woods, (Editor), American Society of Civil Engineers, New York.
- Gibbs, J. F., and T. E. Fumal (1994). Seismic velocities and velocity logs from borehole measurements at seven strong-motion stations that recorded the 1989 Loma Prieta, California, Earthquake, Part IV, *U.S. Geol. Surv. Open-File Rep.* 94-552.
- Graves, R. W. (1998). Three-dimensional finite-difference modeling of the San Andreas Fault: source parameterization and ground-motion levels, *Bull. Seism. Soc. Am.* **88**, 881–897.
- Herrmann, R. B. (1996). Computer Programs in Seismology: 3.0, Saint Louis University, Saint Louis, Missouri.
- Horike, M. (1985). Inversion of phase velocity of long-period microtremor to the S-wave-velocity structure down to the basement in urbanized areas, *J. Phys. Earth* **33**, 59–96.
- ICBO (1997). *1997 Uniform Building Code*, Vol. 2, International Conference of Building Officials, Whittier, California.
- Kawase, H., T. Satoh, T. Iwata, and K. Irikura (1998). S-wave velocity structure in the San Fernando and Santa Monica areas, in *The Effects of Surface Geology on Seismic Motion*, K. Irikura, K. Kudo, H. Okada, and T. Sasatani, (Editors), A. A. Balkema, Rotterdam, 733–740.
- Kilburn, C. (1972). Ground-water hydrology of the Hollister and San Juan Valleys, San Benito County, California, 1913–1968, *U. S. Geol. Surv. Open-File Rep.* 73-0144, 9–13.
- Kramer, S. L. (1996). *Geotechnical Earthquake Engineering*, Prentice-Hall, Upper Saddle River, New Jersey.
- Lacoss, R. T., E. J. Kelly, and M. N. Toksöz (1969). Estimation of seismic noise structure using arrays, *Geophysics* **34**, 21–38.
- Liaw, A. L. (1977). Microseisms in geothermal exploration: studies in Grass Valley, Nevada, *Ph.D. Thesis*, University of California, Berkeley, 168 pp.
- Liu, H.-P., D. M. Boore, W. B. Joyner, D. H. Oppenheimer, R. E. Warrick, W. Zhang, J. C. Hamilton, and Leo T. Brown (2000). Comparison of phase velocities from array measurements of Rayleigh waves associated with microtremor and results calculated from borehole shear-wave velocity profiles, *U. S. Geol. Surv. Open-File Rep.* (in press).
- Malagnini, L., R. B. Herrmann, A. Mercuri, S. Opice, G. Biella, and R. de Franco (1997). Shear-wave velocity structure of sediments from the inversion of explosion-induced Rayleigh waves: comparison with cross-hole measurements, *Bull. Seism. Soc. Am.* **87**, 1413–1421.
- Milana, G., S. Barba, E. Del Pezzo, and E. Zambonelli (1996). Site response from ambient noise measurements: new perspective from an array study in Central Italy, *Bull. Seism. Soc. Am.* **86**, 320–328.
- NEHRP (1997). *NEHRP Recommended Provisions for Seismic Regulations for New Buildings and Other Structures, Part 1: Provisions*, Building Seismic Safety Council, Washington, D. C.
- Oppenheimer, D. H., and H. M. Iyer (1980). Frequency-wavenumber analysis of geothermal microseisms at Norris Geyser basin, Yellowstone National Park, Wyoming, *Geophysics* **45**, 952–963.
- Steidl, J. H., A. G. Turmarkin, and R. J. Archuleta (1996). What is a reference site? *Bull. Seism. Soc. Am.* **86**, 1733–1748.
- Stokoe, K. H. II, and S. Nazarian (1985). Use of Rayleigh waves in liquefaction studies, in *Proc. Conf. on Measurement and Use of Shear Wave Velocity for Evaluating Dynamic Soil Properties*, Denver, Colorado, 1 May 1985, R. D. Woods, (Editors), American Society of Civil Engineers, New York.
- Stokoe, K. H. II, S. G. Wright, J. A. Bay, and J. M. Roesset (1994). Characterization of geotechnical sites by SASW method, in *Geophysical Characterization of Sites*, R. D. Woods (Editors), A. A. Balkema, Rotterdam, 15–25.
- Yamamizu, F., and N. Goto (1978). Direct measurement of seismic wave velocities in deep soil deposits, in *Proc. 5th Japan Earthquake Engineering Symposium*, 329–336.
- Yamamizu, F., H. Takahashi, N. Goto, and Y. Ohta (1981). Shear wave velocities in deep soil deposits. III: Measurements in the borehole of the Fuchu Observatory to the depth of 2,750 m and a summary of the results, *ZISIN, J. Seism. Soc. Japan*, 465–479.

## Appendix

### Theoretical Modeling Results

We gain insight into our experimental results by modeling using synthetic ground noise. We generate synthetic plane surface waves from a single direction as follows: A uniformly distributed random-number generator first produces a time-series  $g(t)$ ; let  $G(\omega) = F[g(t)]$ . The synthetic ground noise at station  $j$  is given by

$$n_j(t) = F^{-1} \{ G(\omega)L(\omega)\exp[i\omega(s_x^{(1)} x_j + s_y^{(1)} y_j)] \},$$

$$j = 1, 2, \dots, 10, \quad (\text{A1})$$

where  $F$  and  $F^{-1}$  denote Fourier and inverse Fourier transforms,  $L(\omega)$  is a low-pass filter, and  $(s_x^{(1)}, s_y^{(1)})$  is an assigned slowness vector.

Synthetic ground noise simulating time-uncorrelated plane surface waves coming from two directions are given by

$$\begin{aligned}
 n_j(t) = & \frac{w^{(1)}}{2\pi} \int_{-\infty}^{\infty} G^{(1)}(\omega)L(\omega)\exp[i\omega(s_x^{(1)}x_j + s_y^{(1)}y_j - t)]d\omega \\
 & + \frac{w^{(2)}}{2\pi} \int_{-\infty}^{\infty} G^{(2)}(\omega)L(\omega)\exp[i\omega(s_x^{(2)}x_j + s_y^{(2)}y_j - t)]d\omega, \\
 & j = 1, 2, \dots, 10, \quad (A2)
 \end{aligned}$$

where  $g^{(1)}(t)$  and  $g^{(2)}(t)$  are two independent random time-series,  $G^{(1)}(\omega) = F[g^{(1)}(t)]$ ,  $G^{(2)}(\omega) = F[g^{(2)}(t)]$ ,  $(s_x^{(1)}, s_y^{(1)})$  and  $(s_x^{(2)}, s_y^{(2)})$  are assigned slowness vectors, and  $w^{(1)}$  and  $w^{(2)}$  are weighing factors with  $w^{(1)} + w^{(2)} = 1$ . Multiple plane surface waves coming from more than two directions can be generalized from equation (A2).

Incoherent noise specific to each station can be added to the synthetic ground noise, equation (A1) or equation (A2), by adding a term,

$$\frac{r_j}{2\pi} \int_{-\infty}^{\infty} \Phi_j(\omega)L(\omega)\exp(-i\omega t)d\omega, \quad (A3)$$

to  $n_j(t)$ ,  $j = 1, 2, \dots, 10$ , where  $\phi_1(t), \phi_2(t), \dots, \phi_{10}(t)$  are independent random time-series,  $\Phi_j(\omega) = F[\phi_j(t)]$ , and  $r_1, r_2, \dots, r_{10}$  are scaling constants.

Results obtained from synthetic ground noise follow.

#### Effect of Single Source

We first model the case for a single plane wave. Figure A1 shows the sample results. The array configuration is that of the Garner-Valley array. Circles are mean values of phase velocities from field measurements and the solid curve is the dispersion curve calculated from an earth model. The synthetic ground noise simulates a plane wave traveling at the calculated phase velocity (solid curve) at the indicated frequency from a given back azimuth (indicated on top of each figure); an incoherent noise time series specific to each array element ( $S/N = 10$ ) has been added. (Possible sources of incoherent noise are small animals and wind. Because the wind was dying down when the data were obtained, it is likely that such incoherent noise were small. On the other

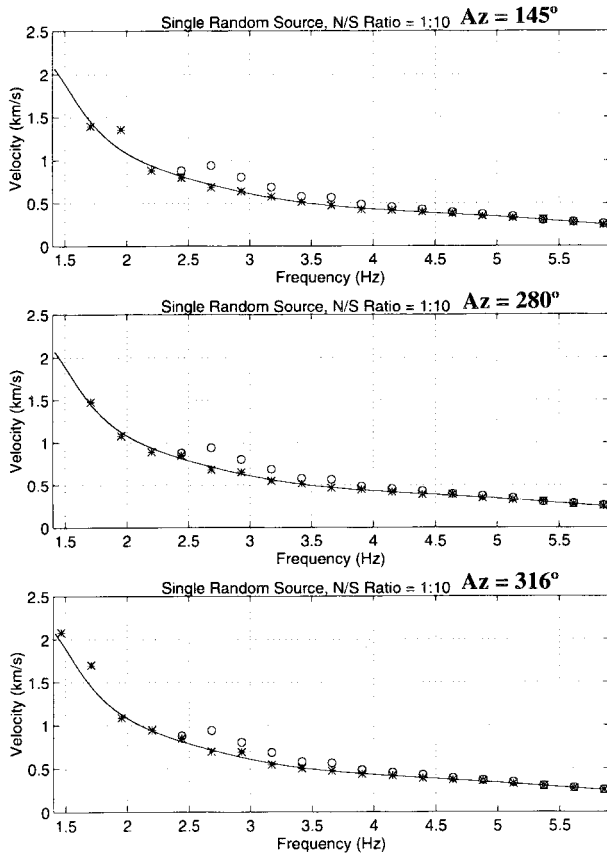


Figure A1. Phase velocities from power-spectral calculation for synthetic ground noise simulating a single plane wave for the Garner-Valley array configuration (stars). The plane wave travels at the calculated phase velocity (solid curve) at the indicated frequency; back azimuth of the plane wave is indicated on top of each plot. Mean values of phase velocities from field measurements (circles) are shown for comparison.

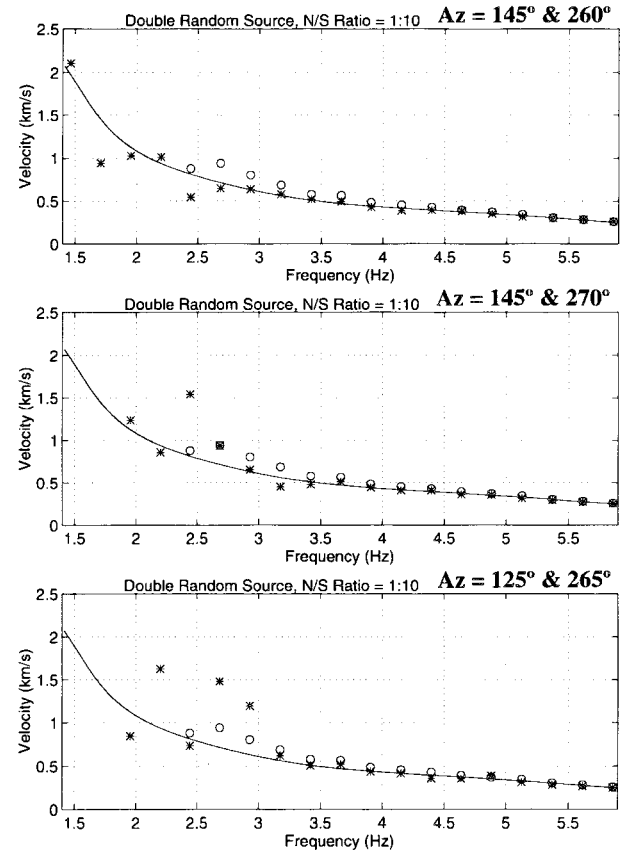


Figure A2. Similar to Figure A1 except that there are two plane waves. Back azimuths of the plane waves are indicated on top of each plot.

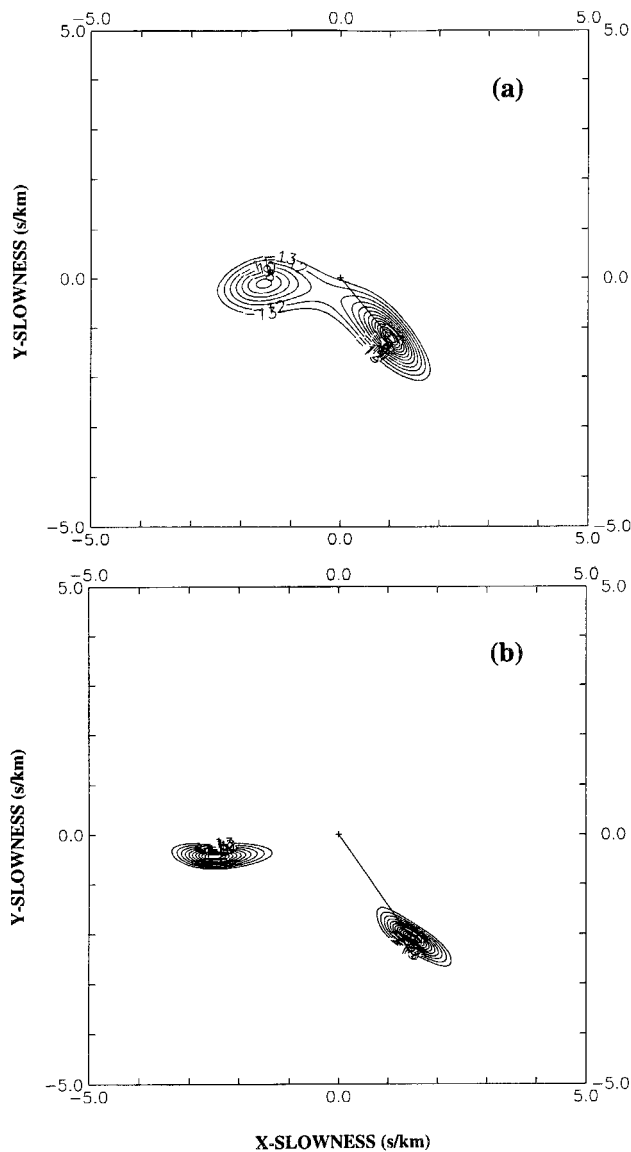


Figure A3. Power spectrum contours (a) at 2.9 Hz, and (b) at 4.4 Hz, for synthetic ground noise simulating two plane waves.

hand, the traffic on the surrounding highways, our coherent noise sources, continued throughout the night.) The stars are phase velocities from power-spectral calculation of the synthetic ground noise. The results show that when the wavelength is 8.5 times the array size (at 1.7 Hz), the phase velocity of a single incoming wave in the presence of local noise can be measured to an accuracy of 3.7% (top figure), 2.0% (middle figure), and 17.5% (bottom figure), respectively.

#### Effect of Multiple Sources

The situation is significantly different when there are two incoming plane waves with equal amplitude traveling with the same slowness but from different back azimuths. Sample results for the configuration of the Garner-Valley array are shown in Figure A2. Power-spectrum contours are shown in Figure A3. At wavelengths greater than 1.8 times the array aperture (at 3.2 Hz), phase velocity from the power-spectral calculations may deviate by a large amount from the phase velocity of the plane waves; the calculated phase velocity is generally biased to a higher value in the bottom two figures. The increase in phase-velocity scatter from synthetic ground noise at low frequencies in Figure A2 is qualitatively similar to those from the observational results in Figure 6. However, the case of two sources with equal amplitude is one of the worst scenarios for array measurement of phase velocities because perfect cancellation or the standing-wave phenomenon can occur. For most of the cases, the actual field situation is likely better than the scenario shown in Figures A2 and A3.

U.S. Geological Survey, MS 977  
 345 Middlefield Road  
 Menlo Park, California 94025  
*liu@usgs.gov*  
*boore@usgs.gov*  
*joyner@usgs.gov*  
*oppen@usgs.gov*  
*jhamilton@usgs.gov*

Manuscript received 7 December 1998.